ECS Journal of Solid State
Science and Technology

On the Impact of Strained PECVD Nitride Layers on Oxide Precipitate Nucleation in Silicon

On the Impact of Strained PECVD Nitride Layers on Oxide Precipitate Nucleation in Silicon

G. Kissinger, *,z **D. Kot, I. Costina, and M. Lisker**

IHP - Leibniz-Institut für innovative Mikroelektronik, 15236 Frankfurt (Oder), Germany

PECVD nitride layers with different layer stress ranging from about 315 MPa to −1735 MPa were deposited on silicon wafers with similar concentration of interstitial oxygen. After a thermal treatment consisting of nucleation at 650°C for 4 h or 8 h followed annealing 780°C 3 h + 1000°C 16 h in nitrogen, the profiles of the oxide precipitate density were investigated. The binding states of hydrogen in the layers was investigated by FTIR. There is a clear effect of the layer stress on oxide precipitate nucleation. The higher the compressive layer stress is the higher is a BMD peak below the front surface. If the nitride layer is removed after the nucleation anneal the BMD peak below the front surface becomes lower. It is possible to model the BMD peak below the surface by vacancy in-diffusion from the silicon/nitride interface. With increasing duration of the nucleation anneal the vacancy injection from the silicon/nitride interface decreases and with increasing compressive layer stress it increases.
 [DOI: 10.1149/2.0061909jss]

Manuscript submitted May 22, 2019; revised manuscript received July 22, 2019. Published August 9, 2019.

Silicon nitride layers belong to the essential components of silicon device technologies. They find their application e. g. in masking, dielectric insulation, passivation, and antireflective coating.[1] Nitride layers can be deposited on silicon by various chemical vapor deposition (CVD) methods or grow thermally in nitrogen containing atmosphere, as e. g. NH_3, whereby the latter methods require much higher temperatures than the former ones.

Nitride layers are well known to affect the intrinsic point defect concentrations in silicon leading to effects like retarded diffusion of B and P, enhanced diffusion of Sb, and shrinkage of oxidation induced stacking faults (OSFs).[2–5] Usually, nitride layers are tensile strained at room temperature. It is assumed that excess vacancies (V) are generated as the result of stress release at the interface. This would explain the observed effects mentioned before very well. Positron beam analysis has confirmed the existence of excess vacancies in the compressed silicon.[6] However, the exact mechanism of vacancy introduction is not fully understood. It is not associated with the thermal growth of a nitride layer because the effect of retarded dopant diffusion lasts for hours compared to the layer growth which stops already after a few minutes when a thickness of 3-5 nm is reached.[7,8] It was also found that deposited nitride layers generate excess vacancies.[4,5,9,10] Models that describe the vacancy injection from the silicon/silicon nitride interface are very rare. In the semi-empirical model of Ref. 8, the vacancy flux from the interface is described via two components, a large flux rapidly decaying lasting for the first few minutes followed by a slowly decreasing flux over several hours. It is assumed that the second component arises from the diffusion of silicon atoms into the silicon nitride layer to relieve the tensile stress.[8]

Investigations of B and P retarded diffusions and OSF shrinkage at 1100°C have shown that the vacancy supersaturation is closely related to the tensile stress level in the silicon nitride layers.[4] It was also found that after removing the nitride layer the effect of enhanced Sb diffusion disappears.[11,12] Retarded B diffusion investigated in the temperature range from 900°C to 1100°C could be related to the vacancy supersaturation caused by compressive stress in the silicon below a tensile strained silicon nitride layer.[10]

Vacancy injection from nitride layers would also affect bulk microdefect (BMD) generation because oxygen precipitation in Czochralski silicon strongly depends on the supersaturation of intrinsic point defects whereby vacancy supersaturation enhances oxygen precipitation and self-interstitial supersaturation retards it.[13,14] Oxide precipitates with and without secondary defects, which are generated for strain relaxation, are usually called BMDs.

It was demonstrated by ab initio calculations that the equilibrium concentrations of vacancies and self-interstitials depend on stress.[15–17] The diffusivities of V and I were also found to be dependent on stress.[18,19] However, the stress levels caused by the silicon nitride layers in the silicon substrate are several orders of magnitude too low to effectively influence the solubility of the intrinsic point defects.

During high temperature (1250°C and 1175°C) rapid thermal annealing (RTA) of silicon covered with deposited nitride layers it was found that N diffuses from nitride layers into silicon and increases the oxide precipitate density.[9] Similar effects were observed after high temperature furnace annealing of wafers covered with silicon nitride layers in Refs. 20–27.

In the work presented here, we have investigated the impact of silicon nitride layers with different layer stress deposited by plasma enhanced chemical vapordeposition (PECVD) on oxide precipitate nucleation at 650°C. The effects caused by nitride layers in this temperature range are still unknown. The PECVD nitride layers used here were compressively as well as tensile strained. This was expected to help to further elucidate the generation mechanism of intrinsic point defects. We used simulation models in order to confirm the conclusions drawn from the experiments.

Experimental

The silicon wafers used for the experiments were 200 mm in diameter, 725 µm thick, B-doped with a resistivity of about 10 Ωcm and a concentration of interstitial oxygen of 6.3×10^{17} cm^{-3} (conversion factor 2.45×10^{17} cm^{-2}). Silicon nitride layers were deposited from the gas phase at about 380°C by PECVD (plasma enhanced chemical vapor deposition) on the front side of the wafers. The layer stress was adjusted to values between 315.5 MPa (tensile) and − 1734.7 MPa (compressive) and the layer thickness was between 569 nm and 747 nm. The layer stress is controllable by the radio frequency (RF) power during the deposition. Higher RF power means more compressive stress. For the layer with the tensile stress of +315 MPa the RF power was set to 600 W and for the layer with the most compressive stress the RF power was adjusted to 1700 W. The dependence of the stress in relation to the RF power is quite linear. All the other the recipe parameters, like pressure, silane and ammonia flow, were kept constant. This allowed us to investigate the impact of tensile and compressive layer stress on the oxygen precipitation and on the generation of excess vacancies from the interface silicon/silicon nitride. In Table I, all thicknesses and layer stresses of the PECVD nitride layers, the RF power, and the initial concentrations of interstitial oxygen of the substrate wafers are summarized. For reference purposes, one wafer was left without nitride layer. The layer stress was measured using a FSM 128 stress and wafer bow/warp measurement system and calculated according to Stoney's equation.[28]

*Electrochemical Society Member.
zE-mail: gkissinger@ihp-microelectronics.com

Table I. Interstitial oxygen concentration of the silicon substrate, RF power during deposition, layer stress and thickness of the PECVD nitride layers.

O_i (10^{17} cm^{-3})	RF power (W)	Average layer stress (MPa)	Average layer thickness (nm)
6.3	–	no layer	0
6.3	600	315.5	689
6.3	900	−53.9	747
6.3	1300	−886.5	682
6.3	1700	−1734.7	569

The wafers were cut into pieces of 3 cm × 3 cm. Then, nucleation anneals at 650°C for 4 h or 8 h in nitrogen were carried out on such samples. After nucleation annealing, a so-called BMD test consisting of an anneal at 780°C for 3h in N_2 for stabilization of the oxide precipitate nuclei and a growth anneal at 1000°C for 16h in N_2 were carried out. This is necessary to grow the oxide precipitate nuclei to sizes above the detection limit of the analysis method.

The BMD density was determined by preferential etching of (110) cleavage planes perpendicular to the (100) wafer surface using the Secco etchant.[29] Depth profiles of the BMD density were generated by measuring the etch pit density across the cleavage plane.

The hydrogen content of the nitride layers was analyzed after the different thermal steps by Fourier transform infrared (FTIR) spectrometry. The spectra were recorded against silicon samples of the same wafer without nitride layer using a resolution of 4 cm^{-1} and an aperture of 1 mm. A Bruker Vertex 80v was used for the measurements.

The nitrogen content was determined by XPS depth profiling, performed in an Ulvac-PHI VersaProbe II instrument equipped with a monochromatic Al K-Alpha X-ray source with a photoelectron take-off angle of 45°, a hemispherical analyzer and Argon ion gun. A dual-beam charge neutralizer (8 eV Ar^+ and 10 eV-electron beam) was used to compensate the charge-up effect. The profiles were acquired by alternatively eroding the surface with a Ar^+ beam (1keV, 2 mm × 2 mm) followed by Si2p and N1s spectra measurement in the center of the crater. The quantification was performed by using the Multipak-Software. The sensitivity factors from Software databank were adjusted with a SiN calibration sample.

In order to find out if the deposition of the PECVD nitride layers lead to a hydrogen-rich layer at the surface of the silicon substrate below the nitride, caused by plasma related damage, hydrogen depth profiles were measured by time-of-flight secondary ion mass spectrometry (ToF-SIMS) in a ToF-SIMS V mass spectrometer from IONTOF. Cesium sputtering was used, and H^- ions were detected since the H^- signal is more sensitive than the H^+ signal. The depth profiles were acquired by sputtering with a Cs^+ ion beam with an energy of 500 eV over a 300 × 300 μm^2 area and analyzing with a Bi^{1+} beam with an energy of 25 keV over a 100 × 100 μm^2 area in the center of the crater produced by the cesium beam. The hydrogen quantification was performed by using the relative sensitivity factors obtained from an implanted standard sample with a known dose of 10^{16} atoms/cm^2.

Experimental Results

In the beginning, we compare the FTIR spectra of the as-deposited nitride layers with different layer stress. In all spectra, shown in Fig. 1, we can find three absorption bands, the Si-N stretch mode between 843–870 cm^{-1}, the Si-H stretch mode between 2170–2183 cm^{-1}, and the N-H stretch mode between 3316–3358 cm^{-1}. These are usually found in PECVD silicon nitride layers.[30–32] It can be seen in Fig. 1 that the maximum absorption coefficients of the Si-H and N-H modes are different. We used the conversion coefficients of Demichelis et al.[30] and calculated the densities of Si-H and N-H bonds. The results shown in Fig. 2 (top left) demonstrate that with increasing compressive stress the concentration of N-H bonds increases and the concentration of Si-H bonds decreases. This is well in agreement with Ref. 31 and due to the increasing RF power for deposition of layers with increasing compressive stress.

In order to find out what happens to the hydrogen during the thermal treatments, we recorded FTIR spectra after the nucleation anneal and after the growth anneal at 1000°C. The corresponding results can be also found in Fig. 2. Because the absorption spectra after 4 h and 8 h of nucleation annealing are similar only the results after 4 h of nucleation are shown here. It can be seen that only minor changes of the concentrations of Si-H and N-H bonds take place during the nucleation anneal at 650°C. This becomes also obvious if the total H concentrations, which are the sums of Si-H and N-H bond densities, are compared (Fig. 2 bottom right). During growth annealing most of the hydrogen evaporates from the layer. In the layers with the two highest values of compressive stress, a small amount of N-H bonds is remaining whereas Si-H is extremely low in all samples after growth annealing at 1000°C for 16 h. The total remaining hydrogen after the growth anneal is decreasing with decreasing compressive layer stress.

Figure 3 shows the composition of the PECVD nitride layers measured by XPS. It can be seen that all layers are sub-stoichiometric with respect to nitrogen. With increasing compressive stress the nitrogen content increases and seems to saturate at 48.4 at% of nitrogen.

Because hydrogen can affect oxygen precipitation, depth profiles of hydrogen were measured by ToF-SIMS after removal of the nitride layers. Sopori et al. detected a 100 nm wide layer of enhanced hydrogen concentration of up to 10^{20} cm^{-3} below the surface. They assume that the hydrogen is trapped there by traps generated by the plasma in the beginning of the PECVD. In our hydrogen depth profiles, shown in Fig. 4, such a layer trapping hydrogen cannot be found. All hydrogen depth profiles are similar and exhibit a hydrogen peak below the surface but only up to a depth of 2 nm. This peak is located in the region of the native oxide and it can be assumed that it is due to the removal of the nitride layer in HF and rinsing in water.

The stress system describing the silicon nitride layers on silicon substrates is fully biaxial. If the layers are compressively strained

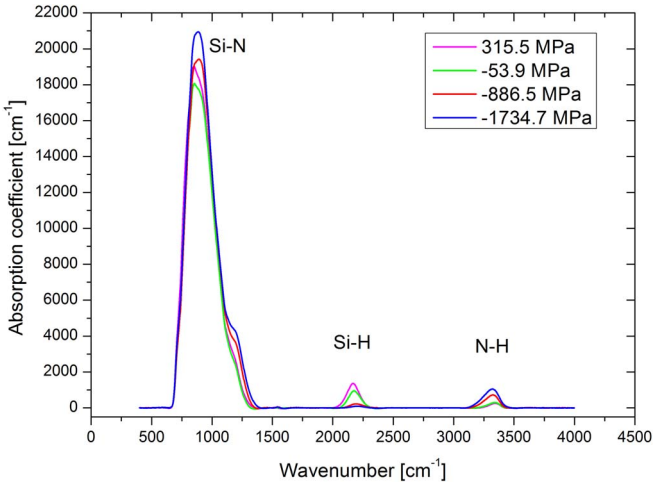

Figure 1. FTIR spectra of as-deposited nitride layers with different average layer stress.

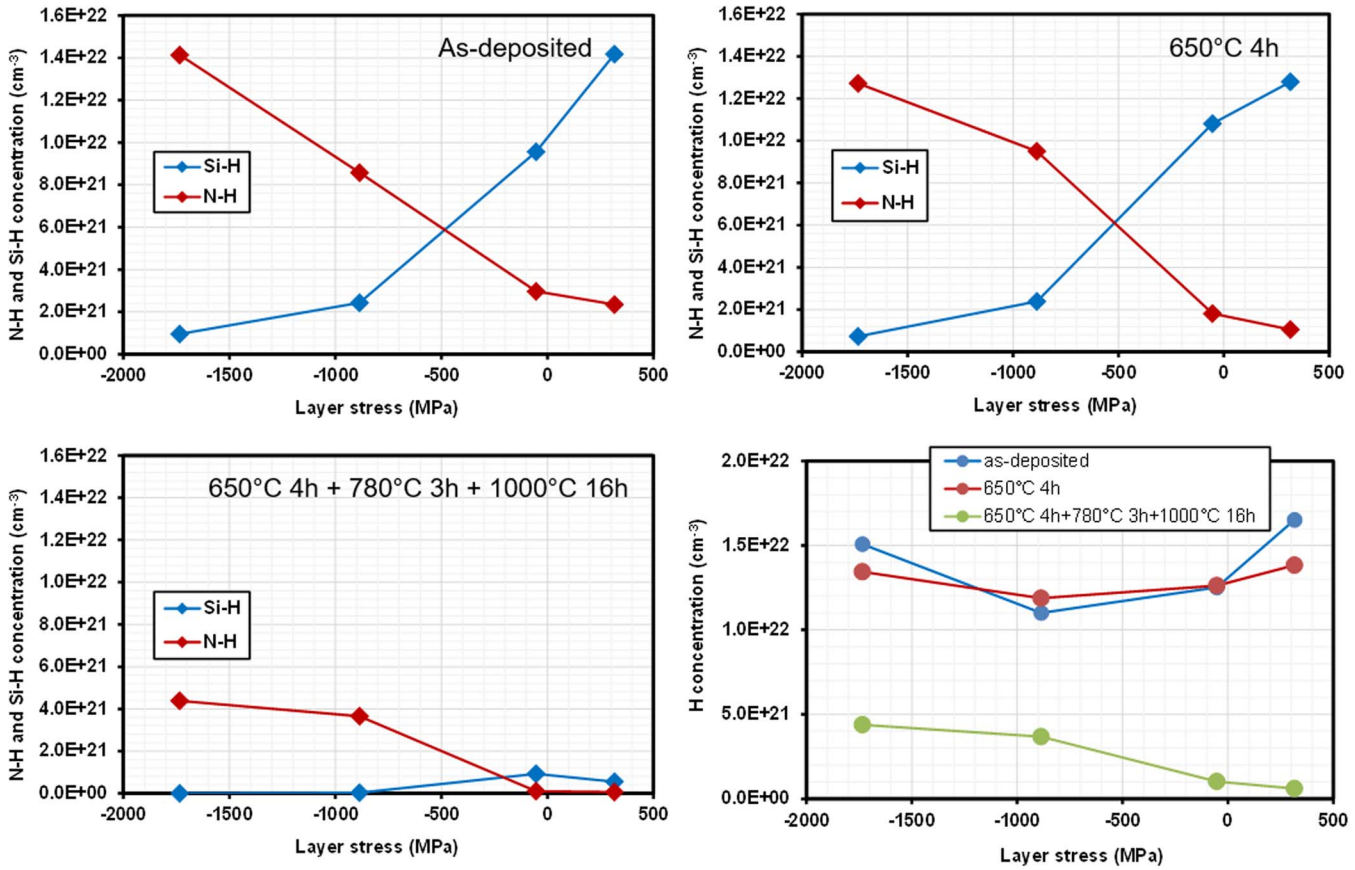

Figure 2. Concentration of N-H and Si-H bonds in the as-deposited nitride layers (top left), after 4 h nucleation anneal at 650°C (top right), and after 4 h nucleation anneal + 780°C 3 h + 1000°C 16 h (bottom left) and changes of the H concentration after different thermal steps (bottom right) all plotted as function of the average layer stress.

the substrate is tensile strained on the front side and compressively strained on the reverse side. For the tensile strained nitride layers it is vice versa. The maximum substrate stress is about three orders of magnitude lower than the layer stress because of the low thickness ratio between layer and silicon wafer.[35]

The depth profiles of the BMD density in silicon covered by nitride layers with different layer stress after 650°C 4 h followed by 780°C 3 h and 1000°C 16 h in N_2 are shown in Fig. 5. One of the samples was an as-grown wafer without nitride layer. This wafer possesses a flat BMD profile. All wafers covered by nitride layers exhibit a BMD density increasing toward the surface. The higher the compressive layer stress, the higher is the peak BMD density below the surface.

In Fig. 6, the depth profiles for 8 h of nucleation time are shown. The profiles also possess a BMD peak below the surface but the BMD densities are higher and the slope reaches deeper regions of the bulk. The wafer without nitride layer has a flat profile but with higher BMD density compared to 4 h of nucleation.

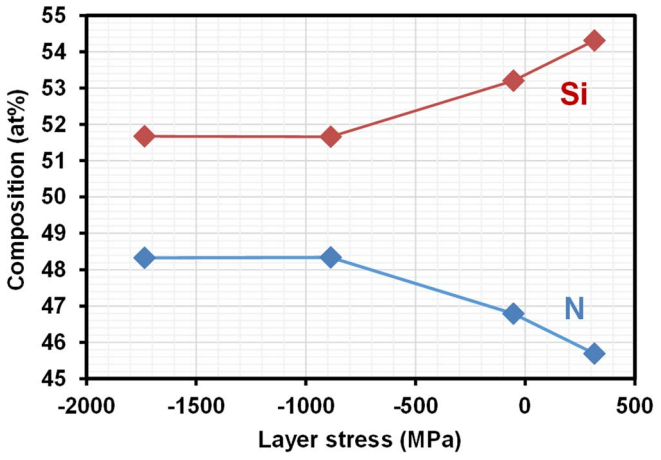

Figure 3. Composition of the PECVD silicon nitride layers plotted as function of the layer stress.

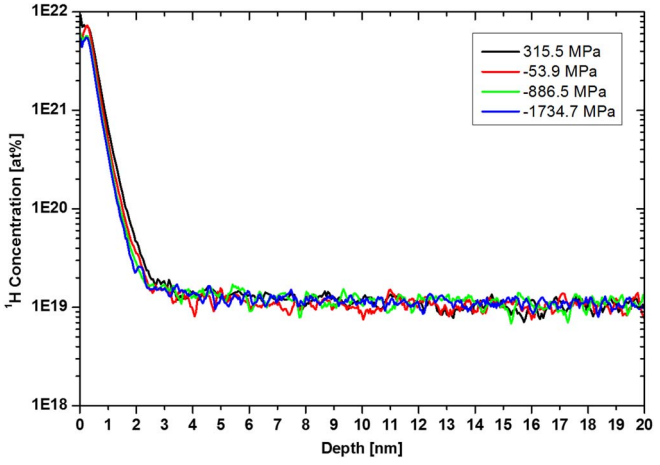

Figure 4. Hydrogen depth profiles of the PECVD silicon nitride layers deposited with different layer stress.

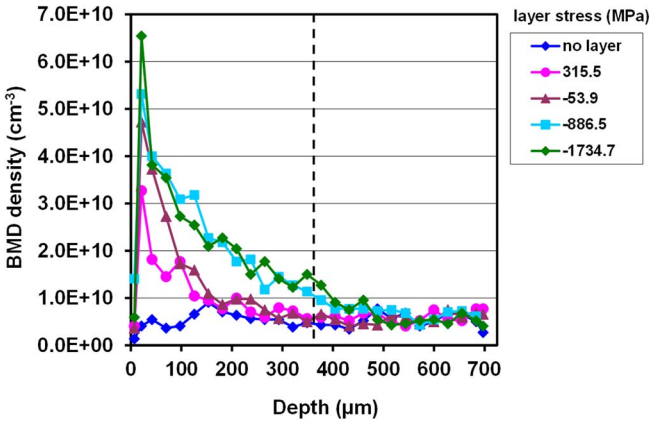

Figure 5. BMD density depth profiles in silicon covered by nitride layers with different layer stress after 650°C 4 h followed by 780°C 3 h and 1000°C 16 h in N_2.

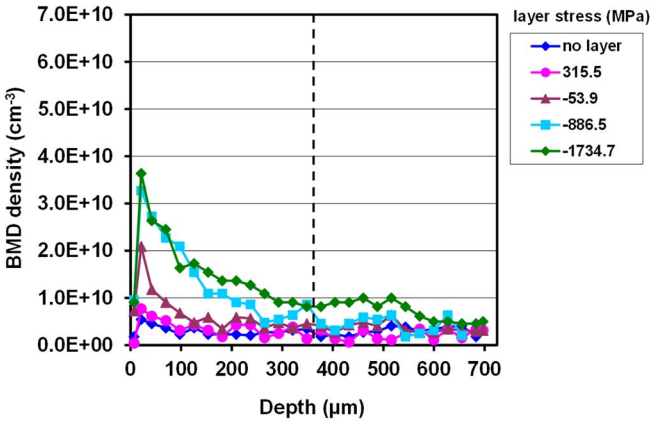

Figure 7. BMD density depth profiles in silicon covered by nitride layers with different layer stress after 650°C 4 h followed by 780°C 3 h and 1000°C 16 h in N_2. The nitride layer was removed after annealing at 650°C.

In order to find out what the effect of the layers during the growth anneal is, in a second set of experiments the silicon nitride layers were etched off after nucleation annealing. The resulting BMD depth profiles for 4 h and 8 h of nucleation can be found in Figs. 7 and 8, respectively. Comparing them with Figs. 5 and 6, it can be seen that the BMD densities are lower if the nitride layers are removed after nucleation annealing. Especially, for 8 h nucleation it can be seen that the BMD density decreases faster toward the bulk.

In Fig. 9, the maximum BMD densities of the four depth profiles are compared. It can be seen that any of the nitride layers on top of the silicon wafers leads to an increased BMD density compared to the bare wafer. With increasing compressive layer stress, the BMD density increases in all types of experiments. As expected, the longer duration of nucleation has generated higher BMD densities. It also becomes obvious that the removal of the nitride layer resulted in lower BMD densities.

Discussion of Experimental Results

We first want to discuss if hydrogen incorporated into the PECVD nitride layers could cause the observed BMD depth profiles. Hydrogen is known to enhance the diffusivity of interstitial oxygen[36] and therefore it could affect the nucleation rate which is proportional to the diffusivity of interstitial oxygen as will be shown later. If hydrogen would diffuse in from the interface nitride layer/silicon, it would be feasible that the observed BMD profiles could be explained in this way. Prerequisite would be that the hydrogen in-diffusion is different for the different layers investigated here. The results of the ToF-SIMS measurement in Fig. 4 are very similar for all nitride layers and with very high probability the hydrogen stems from the layer removal process.

According to the model of Sopori et al.[33,34] a 100 nm surface layer in the silicon substrate with hydrogen trapped during the layer deposition process is necessary for hydrogen in-diffusion into the silicon substrate. The trapped hydrogen would be released during subsequent anneals at temperatures above the layer deposition temperature and can diffuse into the substrate. Such a layer of trapped hydrogen was not detected in our substrates after layer deposition. Furthermore, the shape of the BMD profiles observed do not correspond to the shape as it would be generated by the H-trapping model of Sopori et al.[33,34]

The hydrogen in the layers is well known to be released from the layer surface during anneals at temperatures higher than the temperature of layer deposition.[37–39] The release was monitored by a rest gas analysis and thermal desorption spectroscopy.[37] This leads to an irreversible built-up of more tensile stress in the layers.[37–39] This irreversible increase of tensile stress was shown to be proportional to the reduction of hydrogen. The proportionality constant describes the volume change per evolution of two hydrogen atoms and decreases with increasing temperature of layer deposition.[38] An estimation of the increase of tensile stress due to the released hydrogen concentration according to Hughey and Cook[38] gave values in the range 200–400 MPa for the 1000°C growth anneal. Compared to the

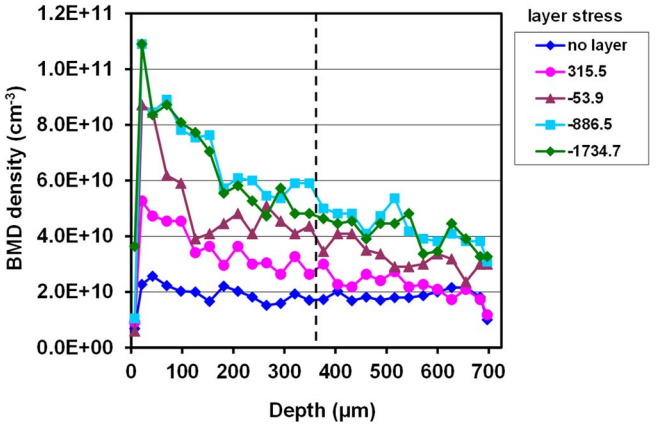

Figure 6. BMD density depth profiles in silicon covered by nitride layers with different layer stress after 650°C 8 h followed by 780°C 3 h and 1000°C 16 h in N_2.

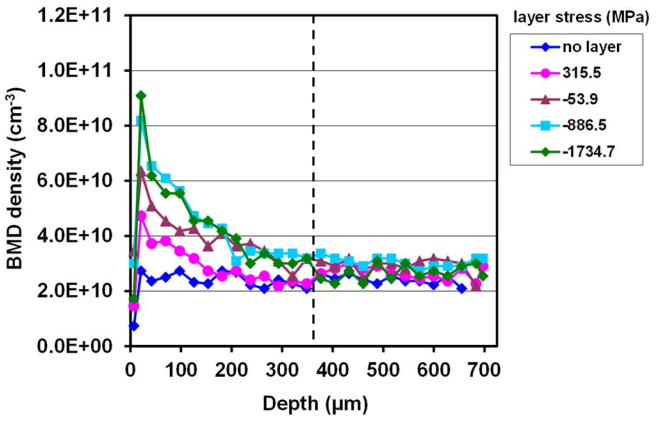

Figure 8. BMD density depth profiles in silicon covered by nitride layers with different layer stress after 650°C 8 h followed by 780°C 3 h and 1000°C 16 h in N_2. The nitride layer was removed after annealing at 650°C.

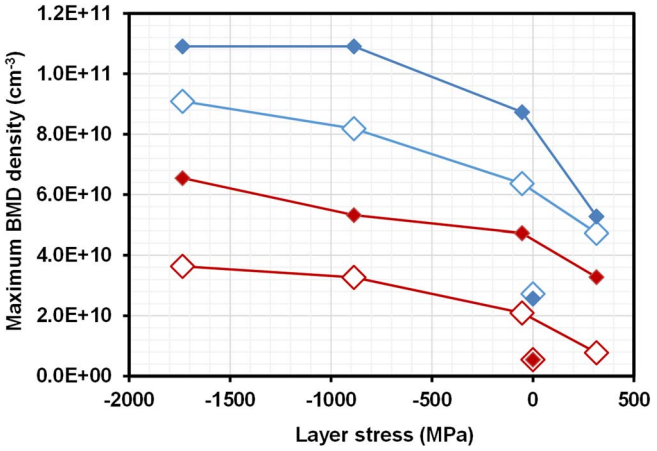

Figure 9. Maximum BMD density in silicon covered by nitride layers with different layer stress after 650°C 4 h (red) and 650°C 8 h (blue) both followed by 780°C 3 h and 1000°C 16 h in N_2. The results with (empty diamonds) and without (full diamonds) removal of the nitride layer after annealing at 650°C are compared.

initial layer stress which is compressive in three cases the full process would lead to compressive stress in only two cases. For the 650°C nucleation anneal the increase of tensile stress would be negligible compared to the initial stress. This is mainly due to the relatively low impact of the 650°C anneal on the hydrogen concentration shown in Fig. 2.

All BMD depth profiles (Figs. 5–8) indicate that a species originating from or induced by the silicon nitride layer is diffusing into the silicon wafer during nucleation as well as during growth annealing enhancing oxygen precipitation. This species could be hydrogen, nitrogen or vacancies. The arguments in the beginning of this section speak against hydrogen because we cannot find a layer with trapped hydrogen serving for hydrogen diffusion into the silicon substrate and because the hydrogen profiles measured are very similar. In addition to this, the total remaining hydrogen in the layers is highest for the wafers with highest BMD enhancement.

Nitrogen is also known to enhance oxygen precipitation.[40] It was found to diffuse into silicon from nitride layers during RTA at high temperature.[9] However, the diffusivity of nitrogen at 650°C is very low.[41] Therefore, the observed BMD profiles cannot be explained by nitrogen in-diffusion. At 1000°C, the diffusivity of nitrogen is much higher. However, on some of the samples we removed the nitride layer after annealing at 650°C and received a strong effect on oxygen precipitation. So nitrogen in-diffusion cannot be regarded as being important to explain the observed results of oxide precipitate nucleation.

The remaining candidate for the in-diffusing species are silicon vacancies. Vacancies are known to enhance oxide precipitate nucleation[13,14] and as described above deposited silicon nitride layers are assumed to generate vacancies because several authors found that boron diffusion is retarded below such layers.[4,5,10] In all these publications, the deposited nitride layers investigated were only tensile stressed. So it is easily understood that due to the tensile stress in the layer and the compressive stress in the silicon substrate silicon atoms from the substrate can be absorbed by the nitride layer for strain relief thus generating silicon vacancies.[4] It was also found that the degree of vacancy supersaturation is dependent on the stress level.[4] Although, the results are usually discussed in this way the mechanism of vacancy generation is not well understood.[8] The results of our work would suggest that with increasing compressive layer stress the vacancy supersaturation would increase. This does not fit into the usual scheme of explanation. An absorption of silicon atoms by the nitride layer for stoichiometric reasons seems also unlikely because it is the nitrogen which is sub-stoichiometric and not the silicon.

In an earlier work, Sopori et al. proposed a hydrogen diffusion mechanism involving {V-H} complex formation.[42] Such process would be also influenced by the concentration of interstitial oxygen as shown in Ref. 42.

Modeling

Vacancies are the most likely candidate for the in-diffusing species in spite of the not well understood mechanism of their generation. Therefore, we try to model the BMD profiles applying a usual basic model which was also used in Ref. 43 to describe interstitial injection from PECVD oxide layers on silicon. It is described here briefly for the case of vacancy injection. The profiles of intrinsic point defects were modeled by including both diffusivity and solubility of the intrinsic point defects and the Frenkel pair equilibrium.[43–46] Then, the change of vacancy V and self-interstitial I concentrations as a function of time t and depth x would be

$$\frac{\partial}{\partial t}C_{V,I}(x,t) = \frac{\partial}{\partial x}\left[D_{V,I}\frac{\partial}{\partial x}C_{V,I}(x,t)\right] - k_{IV}(x,t) \times \left[C_I(x,t)\,C_V(x,t) - C_I^{eq}(x,t)\,C_V^{eq}(x,t)\right] \quad [1]$$

with

$$k_{IV}(x,t) = \frac{4\pi r_c}{\Omega C_{Si}}(D_I + D_V) \quad [2]$$

Here,[36] $D_{V,I}$ are the diffusivities of vacancies and interstitials, $C_{V,I}$ are their concentrations, and $C_{V,I}^{eq}$ are their equilibrium concentrations. From the atomic density of silicon $C_{Si} = 5 \times 10^{22}\text{cm}^{-3}$, the capture radius $r_c = 10^{-7}$cm, and the volume of the silicon unit cell $\Omega = 2.002 \times 10^{-23}\text{cm}^3$ the Frenkel pair reaction constant k_{IV} can be obtained. The energy barrier of the Frenkel pair reaction was assumed to be zero.

The temperature was kept at 650°C for 4 h or 8 h. The initial concentration of intrinsic point defects was set to their equilibrium values $C_{V,I}(x, 0\text{s}) = C_{V,I}^{eq}$. Here, we used two modeling versions. In one model, Dirichlet boundary conditions were used with $C_{V,I}(725\mu\text{m}, t) = C_{V,I}^{eq}(T)$ at the reverse surface, and $C_I(0\mu\text{m}, t) = C_I^{eq}(T)$ and $C_V(0\mu\text{m}, t) = S \cdot C_V^{eq}(T)$ at the front surface. The vacancy supersaturation S at the interface silicon/silicon nitride, assumed to be constant, is as follows

$$S = C_V(T)/C_V^{eq}(T). \quad [3]$$

In a second model, a vacancy source g of the following type

$$-\vec{n}\left(-D_V\frac{\partial}{\partial x}C_V\right) = g \quad [4]$$

was implemented on the front surface instead of assuming a constant vacancy supersaturation.

Because the result of this model are profiles of intrinsic point defects we need transform them into BMD profiles. This can be done via the empirical relation

$$N = a \cdot \left(C_V/10^{13}\right)^3 \cdot \left(C_{Oi}/10^{17}\right)^6 \quad [5]$$

which can be assumed when the BMD density is measured after 780°C 3 h and 1000°C 16 h.[43] The constant a is a fit factor. In our case the concentration of interstitial oxygen C_{Oi} is constant and can be included into a. This way of modeling will not take into account the out-diffusion of oxygen during growth annealing at 1000°C for 16 h and therefore the decrease of the BMD density below the surface.

With the help of modeling and adjustment to experimental data, we intended to determine the diffusion coefficient and supersaturation of vacancies, and the vacancy injection from the interface.

In order to confirm if the vacancy supersaturations obtained from modelling would be suitable to explain the BMD nucleation the time dependent vacancy supersaturations in the depth of maximum BMD density were inserted into a simplified model for nucleation oxide precipitates based on classical nucleation theory. It was assumed that the

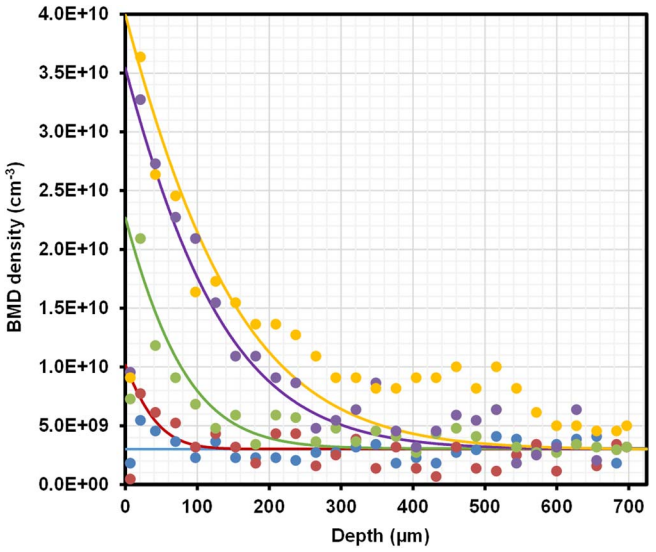

Figure 10. Comparison of modeled (lines)and measured (dots) BMD depth profiles in silicon covered by nitride layers with different layer stress after annealing at 650°C 4 h followed by 780°C 3 h and 1000°C 16 h in N_2. Blue without layer, red 315.5 MPa, green −53.9 MPa, purple −886.5 MPa, and yellow −1734.7 MPa layer stress. The nitride layer was removed after annealing at 650°C.

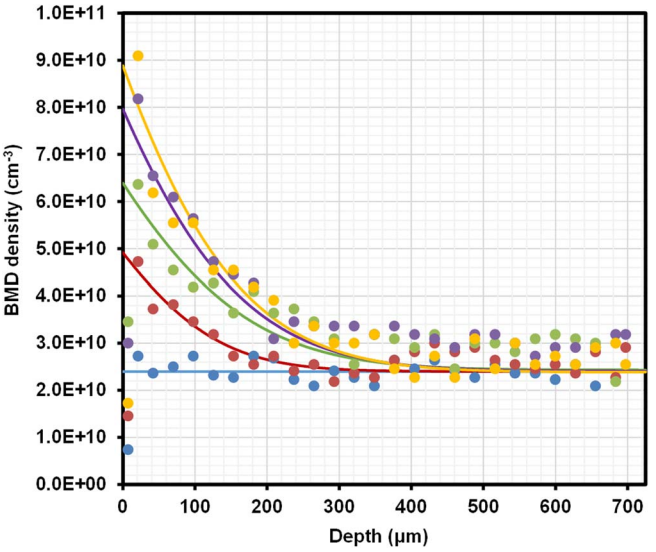

Figure 11. Comparison of modeled (lines)and measured (dots) BMD depth profiles in silicon covered by nitride layers with different layer stress after annealing at 650°C 8 h followed by 780°C 3 h and 1000°C 16 h in N_2. Blue without layer, red 315.5 MPa, green −53.9 MPa, purple −886.5 MPa, and yellow −1734.7 MPa layer stress. The nitride layer was removed after annealing at 650°C.

strain of the spherical oxide precipitates is fully relaxed by absorption of 0.5 vacancies per precipitated oxygen atoms. Then the free energy of formation would be

$$\Delta G = -n\,k\,T\,ln\left[\frac{C_{Oi}}{C_{Oi}^{eq}}S^{0.5}\right] + \left(\frac{36\pi}{C_p^2}\right)^{1/3}\sigma\,n^{2/3} \qquad [6]$$

with n being the number of oxygen atoms in the precipitate, k Boltzman's constant, C_P the density of oxygen atoms in the precipitate, σ the interface energy, and C_{Oi} the initial concentration of interstitial oxygen, and $C_{Oi}^{eq}(T)$ the solubility of interstitial oxygen. The number of oxygen atoms in a critical nucleus n_{crit} is obtained by setting the first derivative of ΔG to zero and resolving for n. The nucleation rate J can be calculated as follows:

$$J = C_{Oi}^2\,exp\left(\frac{-\Delta G_{crit}}{k\,T}\right)\,4\pi\left(\frac{3\,n_{crit}}{4\pi\,C_P}\right)^{2/3}\frac{D_{Oi}}{d}\left(\frac{\Delta G_{crit}}{3\pi\,k\,T\,n_{crit}^2}\right)^{1/2}. \qquad [7]$$

Here, d is the distance of an atomic jump (0.235 nm) and D_{Oi} is the diffusivity of interstitial oxygen. Both, diffusivity and solubility of interstitial oxygen were taken from Mikkelsen.[47]

Results of Modeling

In order to correlate the measured BMD density profiles with the results of modeling, we first determined a by adjusting a calculated profile with $S = 1$ to the measured profile of a wafer without nitride layer. In this case we found $a = 1.22 \times 10^{-8}$ cm^{-24} for 4 h of nucleation and $a = 1.52 \times 10^{-12}$ cm^{-24} for 8 h of nucleation. These values for a were used for all layers of the respective type of nucleation anneal to convert the calculated vacancy concentration into BMD densities with Eq. 5.

In the next step, the modeled profiles of the BMD density were adjusted to the experimental BMD profiles of Figs. 10 and 11 using S and D_V as a fit factors. Figures 10 and 11 demonstrate that the experimental and modeled BMD depth profiles can be well adjusted. This works for both types of boundary conditions, vacancy supersaturation and vacancy source.

In Fig. 12, the resulting vacancy supersaturation at the silicon/nitride interface, the vacancy injection rates, and the diffusivities of vacancies are shown. The upper graphs belong to the model with vacancy supersaturation and the lower graphs belong to the model with vacancy injection as boundary condition. It can be seen that both the vacancy supersaturation and the vacancy injection rate increase with increasing compressive layer stress and decrease with increasing duration of the nucleation anneal. The diffusivities of vacancies, determined here for a temperature of 650°C, are in the range of 1×10^{-8} cm^2/s and they slightly increase with increasing compressive layer stress.

The vacancy concentrations determined here for the nucleation anneals at 650°C, being in the range of 10^5–10^6 cm^{-3}, are very small compared to vacancy concentrations stored by high temperature RTA at 1250°C, being in the range of 10^{13} cm^{-3}.[48] The latter vacancy concentrations are known to enhance the BMD density for subsequent nucleation anneals at 650°C whereas vacancy concentrations stored by RTA at 1100°C, being in the range of a few 10^{12} cm^{-3}, have a weak effect on the BMD density.[49] In order to clarify this, BMD nucleation was modeled. The results in Fig. 13 demonstrate that the maximum BMD densities measured are quite well in agreement with modeling and the surface energies needed to adjust the model to the experiment are reasonable values.

Discussion of Modelling Results

The first results to be discussed are the diffusivities obtained from modeling. The diffusivities of vacancies calculated for 650°C from temperature dependent diffusivities reported in the literature are compared with the average values from this work in Table II. Watkins as well as Frewen and Sinno reported a very high diffusivity for vacancies[45,50] whereas Voronkov et al. claim that there are different vacancy forms, a fast localized species corresponding to the Watkins vacancy and a slow and a fast extended vacancy species.[51,53] The diffusivities found in our works are faster than the slow vacancy of Voronkov and Falster and slower than the Watkins vacancy. In Fig. 14, they are compared with the temperature dependent diffusivities from literature and with experimental diffusivities from RTA from Ref. 45. Similar to the experimentally obtained diffusivities from RTA the diffusivities from this work are located between fast and slow vacancies. The reason for the lower diffusivity could be that part of the

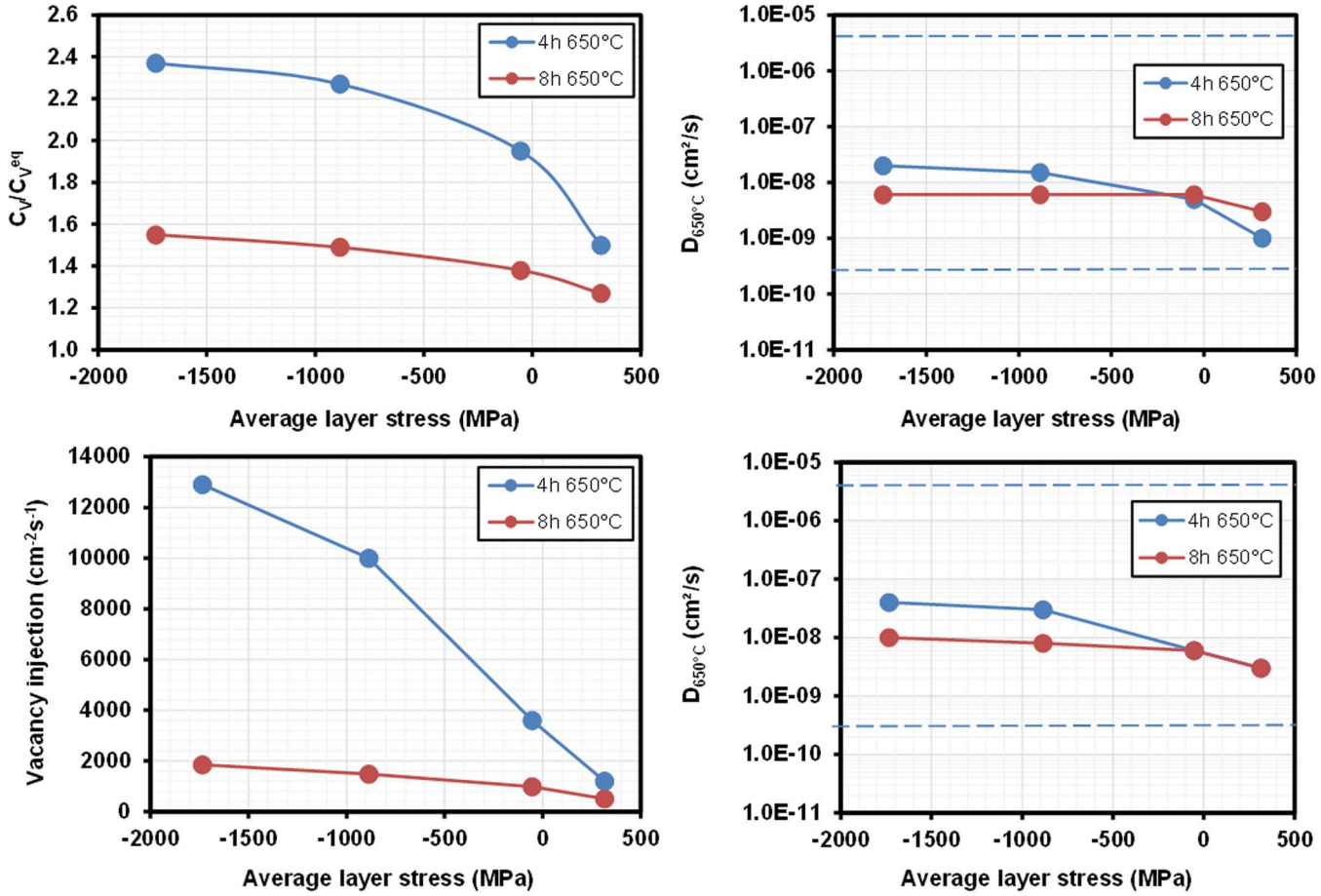

Figure 12. Vacancy injection from the oxide/silicon interface plotted as function of the average layer stress. Vacancy supersaturation at the oxide/silicon interface plotted as function of the average layer stress.

vacancies bind to oxygen. As an example the diffusivity of vacancy-oxygen complexes from Quemener et al. is provided in Table II. It is one order of magnitude lower than that of the slow vacancy. A similar explanation was proposed in Ref. 53. However, in our case with considerable hydrogen concentration in the nitride layers the inner bonds of the vacancies generated at the interface silicon /nitride could be saturated by hydrogen atoms forming $\{V,H_m\}$ with $m = 1$-4. Ab initio calculations have demonstrated that only $\{V,H_1\}$ would be diffusive and its diffusivity would be lower than that of a single vacancy.[42]

Modelling of nucleation and the experimental results have demonstrated that low vacancy concentrations being sufficiently supersaturated can efficiently enhance oxide precipitate nucleation at 650°C. This was a quite unexpected result because until now it was assumed that considerably higher vacancy concentrations are necessary for enhanced oxygen precipitation. These are usually introduced by RTA at 1200°C and higher.[48] We assume that the nucleation enhancement is possible because the diffusive vacancies are available to be built into the precipitate nuclei during annealing at 650°C when they diffuse into the silicon wafer from the silicon/nitride interface. If the 650°C anneal is carried out after a high temperature RTA, the early stages of oxide precipitates are already formed during RTA cooling and the vacancies are bound in VO_n complexes which are mainly VO_4.[54] In

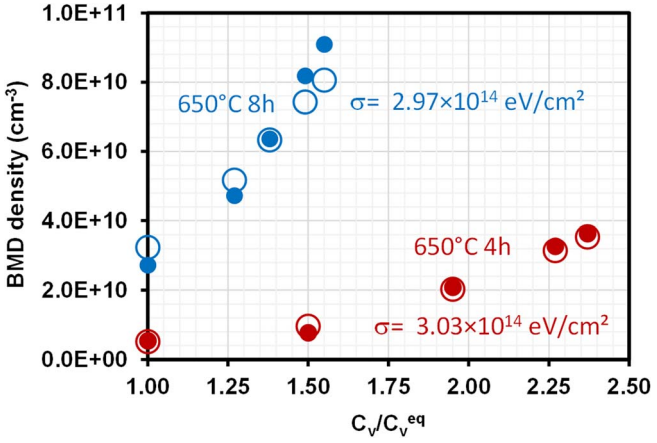

Figure 13. Comparison of measured maximum BMD densities (full circles) with modeled BMD densities at a depth of 19 μm below the surface (open circles) for 4 h of nucleation at 650°C (red symbols) and 8 h of nucleation at 650°C (blue symbols).

Table II. Diffusivities of vacancies at 650°C reported in the literature compared to diffusivities obtained in this work.

Diffusivity at 650°C (cm^{-3}/s)	Reference
4.19×10^{-6}	vacancy Watkins[50]
2.52×10^{-6}	vacancy Frewen and Sinno[45]
2.93×10^{-10}	slow vacancy Voronkov and Falster[51]
1.20×10^{-11}	vacancy-oxygen Quemener et al.[52]
1.0×10^{-8}	average for 4 h 650°C this work
5.3×10^{-9}	average for 8 h 650°C this work

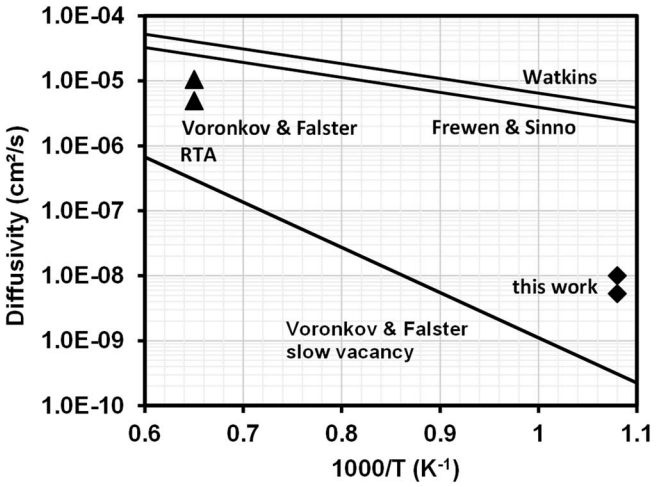

Figure 14. Diffusivities of vacancies from Refs. 5,45,50 plotted as function of the reciprocal temperature. Experimental values from Ref. 51 (full triangles) and this work (full diamonds) are also shown.

other words, oxide precipitate nucleation took place already during RTA cooling and the 650°C anneal first of all stabilizes and grows the existing nuclei in this case.

Conclusions

In in order to investigate the effect of the nitride layer stress on oxide precipitate nucleation, PECVD nitride layers with different layer stress ranging from about 315 MPa to −1735 MPa were deposited on silicon wafers with similar concentration of interstitial oxygen. Wafers with and without nitride layers on the front surface were subjected to nucleation anneals at 650°C for 4 h or 8 h followed by stabilization annealing at 780°C for 3 h and growth annealing at 1000°C for 16 h, all in nitrogen. The conclusions from this work can be summarized as follows.

1. The layers contain hydrogen in different binding states. With increasing compressive layer stress the concentration of the N-H bonds increases, the concentration of the Si-H bonds decreases, and the layers become more silicon rich. All layers are sub-stoichiometric with respect to nitrogen. During annealing at 650°C most of the hydrogen is kept in the nitride layers whereas during the growth anneal at 1000°C it is evaporating to a large extent. The total remaining hydrogen after the growth anneal is decreasing with decreasing compressive layer stress.
2. There is a clear effect of the layer stress on oxide precipitate nucleation. The higher the compressive layer stress is the higher is a BMD peak below the front surface. If the nitride layer is removed after the nucleation anneal the BMD peak below the front surface becomes lower.
3. It is possible to model the BMD peak below the surface by vacancy in-diffusion from the silicon/nitride interface. With increasing duration of the nucleation anneal the vacancy injection decreases and with increasing compressive layer stress it increases.
4. The diffusivity of vacancies obtained from the adjustment of the model to the experimental BMD profiles is lower than Watkins's fast vacancy and higher than Voronkov and Falsters's slow vacancy. It is assumed that the reasons for the reduced diffusivity are the formation of vacancy-oxygen complexes and binding of hydrogen to the vacancies.

The results of this work also raised questions which could not be resolved at this stage. The main question is: Why compressive layer stress leads to generation of vacancies? Most thermal and deposited silicon nitride layers on silicon are tensile strained. In these cases, stress relieve in the compressively strained silicon by vacancy generation seemed reasonable.

Acknowledgment

The authors thank Julia Kitzmann from IHP for the XPS measurements.

ORCID

G. Kissinger https://orcid.org/0000-0002-6492-3117
D. Kot https://orcid.org/0000-0002-7857-5416

References

1. A. E. Kaloyeros, F. A. Jove, J. Goff, and B. Arkles, *ECS J. Solid State Science and Technology*, **6**, P691 (2017).
2. P. Fahey, G. Barbuscia, M. Moslehi, and W. Dutton, *J. Appl. Phys.*, **46**, 784 (1985).
3. S. Mizuo, T. Kusaka, A. Shintani, M. Nanba, and H. Higuchi, *J. Appl. Phys.*, **54**, 3860 (1983).
4. S. T. Ahn, H. W. Kennel, J. D. Plummer, and W. A. Tiller, *J. Appl. Phys.*, **64**, 4914 (1988).
5. K. Osada, Y. Zaitsu, S. Matsumoto, M. Yoshida, E. Arai, and T. Abe, *J. Electrochem. Soc.*, **142**, 202 (1995).
6. S. Matsumoto, K. Osada, Y. Zaitsu, T. Shimizu, E. Arai, S. Tanigawa, and T. Abe, *Defect and Diffusion Forum*, **153–155**, 25 (1998).
7. P. Pichler, Intrinsic point defects, impurities, and their diffusion in silicon, Springer Wien, New York, pp. 186 (2004).
8. M. Hasanuzzaman and Y. M. Haddara, *J. Mat. Sci.: Mater. Electron.*, **19**, 323 (2008).
9. G. Kissinger, D. Kot, J. Dabrowski, T. Grabolla, T. Müller, and A. Sattler, *Phys. Stat. Sol. A*, **214**, 1700236 (2017).
10. Y. Zaitsu, T. Shimizu, J. Takeuchi, S. Matsumoto, M. Yoshida, T. Abe, and E. Arai, *J. Electrochem. Soc.*, **145**, 258 (1998).
11. S. T. Ahn, H. W. Kennel, J. D. Plummer, and W. A. Tiller, *Appl. Phys. Lett.*, **53**, 1593 (1988).
12. P. M. Fahey, P. B. Griffin, and J. D. Plummer, *Reviews of Modern Physics*, **61**, 289 (1989).
13. J. Vanhellemont and C. Claeys, *J. Appl. Phys.*, **62**, 3960 (1987), Erratum *J. Appl. Phys.*, **71**, 1073 (1992).
14. S. M. Hu, *Appl. Phys. Lett.*, **48**, 115 (1986).
15. A. Antonelli and J. Bernholc, *Phys. Rev. B*, **40**, 10643 (1989).
16. K. Sueoka, E. Kamiyama, J. Vanhellemont, and K. Nakamura, *ECS Solid State Lett.*, **3**(6), P69 (2014).
17. K. Nakamura, R. Suewaka, and B. Ko, *ECS Solid State Letters*, **3**(3), N5 (2014).
18. M. J. Aziz, Y. Zhao, H.-J. Gossmann, S. Mitha, S. P. Smith, and D. Schiferl, *Phys. Rev. B*, **73**, 054101 (2006).
19. P. Pochet and D. Caliste, *Mat. Sci. in Semicond. Proc.*, **15**, 675 (2012).
20. L. Fu, D. Yang, X. Ma, H. Jiang, and D. Que, *Semicond. Sci. Tech.*, **22**, 1303 (2007).
21. X. Ma, L. Fu, and D. Yang, *Solid State Phenom.*, **178–179**, 249 (2011).
22. H. Nakazawa, M. Ogino, H. Teranishi, Y. Takahashi, and H. Habuka, *Jpn. J. Appl. Phys.*, **53**, 05FJ05 (2014).
23. A. Hara, T. Fukuda, T. Miyabo, and I. Hirai, *Appl. Phys. Lett.*, **54**, 626 (1989).
24. Q. Wang, M. Daggubati, R. Yu, and X. F. Zhang, *Appl. Phys. Lett.*, **88**, 242112 (2006).
25. F. Shimura and R. S. Hockett, *Appl. Phys. Lett.*, **48**, 224 (1986).
26. I. Itoh, Y. Hayamizu, and T. Abe, *Mat. Sci. Eng. B*, **4**, 309 (1989).
27. G. Kissinger, G. Raming, R. Wahlich, and T. Müller, *Physica B*, **407**, 2993 (2012).
28. G. G. Stoney, *Royal Society Proceedings*, **82** No. (A553), 172 (1909).
29. Secco d'Aragona, *J. Electrochem. Soc.*, **119**, 948 (1972).
30. F. Demichelis, F. Giorgis, and C. F. Pirri, *Phil. Mag. B*, **74**, 155 (1996).
31. S. Kobayashi, *World J. Condensed Matter*, **6**, 287 (2016).
32. W. A. Lanford and M. J. Rand, *J. Appl. Phys.*, **49**, 2473 (1978).
33. B. Sopori, *J. Electron. Mat.*, **32**, 1034 (2003).
34. B. Sopori, Y. Zhang, and N. M. Ravindra, *J. Electron. Mat.*, **30**, 1616 (2001).
35. R. J. Jaccodine and W. A. Schlegel, *J. Appl. Phys.*, **37** (1966) 2429.
36. R. C. Newman, J. H. Tucker, A. R. Brown, and S. A. McQuaid, *J. Appl. Phys.*, **70**, 3061 (1991).
37. F. C. Morin, B. Pelletier, E. Laffosse, and L. Plantier, *J. Appl. Phys.*, **114**, 154113 (2013).
38. M. P. Hughey and R. F. Cook, *J. Appl. Phys.*, **97**, 114914 (2005).
39. J. Thurn, R. F. Cook, M. Kamarajugadda, S. P. Bozeman, and L. Sterns, *J. Appl. Phys.*, **95**, 967 (2004).
40. C. Cui, D. Yang, X. Ma, R. Fan, and D. Que, *Phys. Status Solidi A*, **203**, 2370 (2006).
41. I. Itoh, Y. Hayamizu, and T. Abe, *Mater. Sci. Eng. B*, **4**, 309 (1989).
42. B. L. Sopori, X. Deng, J. P. Brenner, A. Rohatgi, P. Sana, S. K. Estreicher, Y. K. Park, and M. A. Robertson, *Solar Energy Materials and Solar Cells*, **41/42**, 159 (1996).
43. G. Kissinger, D. Kot Lisker, and A. Sattler, *ECS J. Solid State Sci. Technol.*, **8**, N79 (2019).
44. G. Kissinger, D. Kot, and W. von Ammon, *ECS J. Solid State Sci. Technol.*, **1**, P269 (2012).
45. T. A. Frewen and T. Sinno, *Appl. Phys. Lett.*, **89**, 191903 (2006).
46. J. Frenkel, *Kinetic theory of liquids*, Oxford Univ. Press, Oxford, 1946.
47. J. C. Mikkelsen Jr,, *Mater. Res. Soc. Symp. Proc.*, **59**, 19 (1986).

48. R. Falster, M. Pagani, D. Gambaro, M. Cornara, M. Olmo, G. Ferrero, P. Pichler, and M. Jacob, *Solid State Phenom.*, **57–58**, 129 (1997).
49. G. Kissinger, Oxygen precipitation in silicon, in: Defects and impurities in silicon materials, ed. by Y. Yoshida and G. Langouche, Springer Japan 2015, pp. 273.
50. G. D. Watkins, *J. Appl. Phys.*, **103**, 106106 (2008).
51. V. V. Voronkov and R. Falster, *Sold State Phenom.*, **205–206**, 157 (2014).
52. V. Quemener, B. Raeissi, F. Herklotz, L. I. Murin, E. V. Monakhov, and B. G. Svensson, *J. Appl. Phys.*, **118**, 135703 (2015).
53. V. V. Voronkov, R. Falster, and P. Pichler, *Appl. Phys. Lett.*, **104**, 032106 (2014).
54. D. Kot, G. Kissinger, J. Dabrowski, and A. Sattler, *ECS J. Solid State Sci. Technol.*, **7**, P707 (2018).